Langmuir

ARTICLE

pubs.acs.org/Langmuir

Recognition Ability of DNA for Carbon Nanotubes Correlates with Their Binding Affinity

Daniel Roxbury,[†] Xiaomin Tu,[‡] Ming Zheng,[‡] and Anand Jagota*[,†]

[†]Department of Chemical Engineering and Bioengineering Program, Lehigh University, Bethlehem, Pennsylvania 18015, United States

[‡]Polymers Division, National Institute of Standards and Technology, Gaithersburg, Maryland 20899, United States

Supporting Information

ABSTRACT: The ability to sort mixtures of carbon nanotubes (CNTs) based on chirality has recently been demonstrated using special short DNA sequences that recognize certain matching CNTs of specific chirality. In this work, we report on a study of the relationship between recognition sequences and the strength of their binding to the recognized CNT. We have chosen the (6,5) CNT and its corresponding DNA recognition sequences for investigation in this study. Binding strength is quantified by studying the kinetics of DNA replacement by a surfactant, which is monitored by following shifts in the absorption spectrum. We find that recognition ability correlates strongly with binding strength thus measured; addition or subtraction of just one base from the recognition sequence can enhance the kinetics of DNA displacement some 20-fold. The surfactant displaces DNA in two steps: a rapid first stage lasting less than a few seconds, followed by progressive removal lasting tens of minutes. The kinetics of the second stage is analyzed to extract activation energies. Fluorescence studies support the finding that the DNA sequence that recognizes the (6,5)-CNT forms a more stable hybrid than its close relatives.

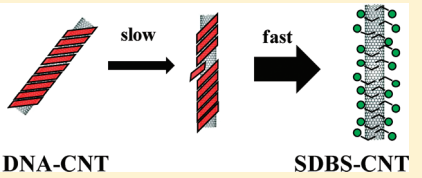

1. INTRODUCTION

Many novel applications for carbon nanotubes (CNTs) have been developed on the basis of their unusual physical and electrical properties.[1−4] However, as-produced, CNTs comprise a variety of chiralities and are clumped together because of their high aspect ratios.[5,6] Solution-based processing has been successful for the effective dispersion of individual CNTs. Several amphiphilic molecules, such as surfactants,[7−9] peptides,[10] and lipids,[11,12] have been shown to adsorb noncovalently on the hydrophobic CNT sidewall, effectively solubilizing the resultant hybrid molecule in an aqueous medium.

Single-stranded DNA (ssDNA) having both a hydrophilic backbone and hydrophobic bases was demonstrated as having CNT-dispersing capabilities,[13] allowing subsequent sorting by diameter and length.[14,15] Atomic force microscopy suggests a helically wrapped structure.[15] More recently, it has been shown that a sequence-specific motif exists whereby particular short ssDNA sequences recognize specific chirality CNTs, permitting their separation from a mixture.[16] These recognition sequence hybrids, which show high selectivity toward their respective chirality CNT, suggest a highly ordered ssDNA secondary structure proposed to be stabilized by base-CNT adsorption as well as by interbase hydrogen bonding.[16−18]

To understand the nature of ssDNA-CNT interactions, it is first useful to consider arrangements formed by individual DNA bases on planar graphite. Overlapping π orbitals are known to cause aromatic bases to stack on aromatic substrates.[19,20] Base adsorption at the graphite−water interface results in the formation of a self-assembled monolayer,[21−23] and the strength of adsorption was found to be in the following order: G > A > T > C.[21] Numerous studies have been performed, through AFM and STM imaging,[23−26] with monolayer-adsorbed DNA bases showing the emergence of a 2D crystalline structure thought to be stabilized by interbase cyclic hydrogen bonds.[24,27,28] Supramolecular structures created at solid−liquid interfaces, composed of guanine, adenine, and mixtures of adenine/thymine and guanine/cytosine, have also been investigated.[23−25,27,29−31] Single base adsorption on a CNT, modeled computationally through thermodynamic integration,[32,33] was found to be in agreement with the base-graphite binding strength order.

Little is known about how or if DNA bases form ordered structures when the bases are linked to form ssDNA or when the surface on which they adsorb is a cylindrical carbon nanotube. Binding strengths for homopolymeric DNA on graphite, investigated through molecular dynamics (MD) simulation peeling,[34] suggest the same trend (G > A > T > C) as measured for individual bases. Contrary to this, experimental values for peeling homopolymer DNA from graphite go as T > A > C.[35] DNA-CNT hybrids composed of DNA strands of less than 10 bases were shown to dissociate thermally in yet another trend: G > C > A > T.[36] Also in this study, binding free energies of entire ssDNA strands to CNTs were argued to increase monotonically with increasing sequence length.

The evidence of DNA-CNT recognition sequences suggests the formation of a highly ordered oligomeric ssDNA arrangement on the CNT. DNA β-barrel structures have been proposed to be an ordered form of ssDNA in which the backbone and bases are both arranged helically on an imaginary cylinder.[16,17] The

Received: February 28, 2011
Revised: May 22, 2011
Published: June 08, 2011

 © 2011 American Chemical Society

interior of the structure is hollow and permits the insertion of a CNT of a specific diameter. The barrels are generally composed of two or more strands of ssDNA wrapped helically and stabilized by interstrand hydrogen bonding between bases. This conformation allows for all of the DNA bases to be adsorbed on the CNT sidewall as well as for base-to-base hydrogen bonding.[37,38]

In this study, we report the results of experiments to probe the binding strength of DNA strands to a specific CNT (6,5). (It was chosen for its natural abundance in the CoMoCAT sample, which significantly reduces the sample preparation burden.) We do so by studying the kinetics of competitive binding for the surface of the CNT between a small surfactant molecule, sodium dodecylbenzene sulfonate (SDBS) that has a high affinity for adsorbing on the CNT sidewall,[39] and the prewrapped DNA. When present in sufficient concentration in the solution, SDBS displaces DNA from the CNT at a characteristic temperature-dependent rate. The exchange process from DNA-covered to SDBS-covered CNTs can be conveniently followed by characteristic shifts in optical absorbance, a solvatochromic effect.[40] Transition-state theory[41] can be used quantitatively to extract activation energies, allowing quantitative comparison among sequences for binding to a given CNT species. We expect that some of the general findings about the relative binding strengths of DNA sequences will apply to other DNA-CNT combinations, which will be studied in future work.

In addition to hybrid dissociation, correlation with CNT dispersion efficiencies was monitored through photoluminescence measurements for various DNA sequences. Furthermore, a surfactant-exchange method was employed to strip DNA off of the CNT to prevent any wrapping effects on the fluorescence intensity.

2. EXPERIMENTAL METHODS

Raw (6,5)-rich (>80%) CoMoCAT carbon nanotubes, obtained from South West NanoTechnologies (SWeNT), and single-stranded DNA, obtained from Integrated DNA Technologies (IDT), in a 1 mg/1 mg weight ratio were sonicated using a Branson probe ultrasonicator for 90 min at 8 W output power in 4 mL of a 2× SSC buffer. All chemicals other than CNT and DNA were purchased from Sigma-Aldrich. The resultant dispersion was centrifuged (Eppendorf microcentrifuge) for 90 min at 13K rpm to precipitate any undispersed CNTs. The extracted supernatant was then fed through size-exclusion columns (2000, 1000, and 300 Å pore sizes, Sepax Technologies) via HPLC (AKTA UPC-10 GE) and fractionated to remove excess DNA and sort CNTs according to length.[14] (See Supporting Information S1 for additional data.) The length of the CNTs used for the majority of the experiments was an SEC fraction of the CNT length range of 250−350 nm, verified by atomic force microscopy (AFM) imaging (Veeco Nanoscope). It turns out that that the kinetics of surfactant exchange depend strongly on length, so the ability to sort them by length is important. The fractions were then exchanged in a 10 mM 7.1 pH phosphate buffer through microcentrifuge filtration (100 kDa cutoff Microcon). (This buffer exchange is required because SDBS is ineffective at the higher salt concentration needed for SEC separation.) Relative concentrations of (6,5) CNTs in solution were verified by optical absorbance at the E_{11} transition (990 nm), and fractions were diluted as such so that $Abs_{990} = 1.0 \pm 0.01$ across samples. A stock solution of 0.2 wt % sodium dodecylbenzene sulfonate (SDBS) was made in the same 10 mM phosphate buffer solution. A volume of 100 μL was preheated in a quartz microcuvette to the desired temperature in a constant-temperature Peltier device (held constant at various temperatures, 20−80 °C) and mixed (by pipet mixing) with equal volumes of the DNA-CNT fraction to obtain an effective SDBS concentration of 0.1 wt % (below the experimentally determined cmc value of 0.223). Because the mass of the cuvette far exceeds that of the injected sample, temperature equilibration after the injection of DNA-CNT is estimated to take less than 5 s. Upon mixing, surfactant exchange was monitored through a time-dependent changing optical absorbance signal (via a Varian Cary 50 UV/vis/NIR spectrophotometer). The time between mixing and the start of the absorbance scan was less than 3 s.

Surface tensions and cmc values of various SDBS/buffer/DNA solutions were estimated by means of a drop counting method. Using a 0.5 mL syringe with a circular tip opening of radius 0.25 mm, the number of drops was counted in various SDBS, sodium deoxycholate (SDC), and DNA concentrations ranging from 0 to 3 wt % in a 10 mM phosphate-buffered solution. The number of drops would increase as the surface tension of the solution decreased to a plateau value (for the case of SDBS, its critical micelle concentration (cmc)).[42] Note that whereas this method cannot be used in this form to estimate the suface tension, it does yield information on the cmc.

HiPCO CNTs (Rice University) were dispersed with ssDNA in the same manner as previously described but in 0.1 M NaCl solution. Without the use of size exclusion, the supernatant was diluted 20-fold before fluorescence measurements were made using a Horiba Jobin Yvon Nanolog-3 spectrofluorometer with a liquid-nitrogen-cooled InGaAs detector. The sample was measured in a 10 mm^2 quartz cuvette. The light source is a 450 W xenon lamp. Both the excitation and emission wavelength were scanned in 10 nm increments with an 8 nm slit. The emission spectra were corrected for the inhomogeneous spectral distributions from the light source and detector. SDC was added to the diluted sample to make a final concentration of 1 wt % to replace the DNA coating with surfactant. Fluorescence intensities were measured and correlated with the dispersion efficiency of the DNA sequences.

3. DNA−SURFACTANT EXCHANGE ON THE CARBON NANOTUBE

Optical absorption spectra from clean, singly dispersed CNTs show prominent peaks due to the semiconducting band gap of nanotubes.[7,9] The positions of these peaks are strongly dependent on the environment of the CNTs.[43] For example, replacing DNA by surfactant causes a solvatochromic shift ascribed to be due to a change in the effective dielectric constant.[40] In this study, we use this fact to monitor the temperature-dependent, kinetically controlled exchange of the surface coverage of a (6,5) chirality CNT from ssDNA to the SDBS surfactant. For this particular CNT, the E_{11} transitions when covered by DNA or SDBS are at 990 and 978 nm, respectively. By using the surfactant as a common reference, and by analyzing the kinetics of its exchange with DNA on the surface of the CNT, our aim is to determine certain characteristics of the relative binding strengths of ssDNA on CNTs.

It was found that by merely increasing the temperature of the solution the DNA−surfactant exchange could be sped up dramatically. Figure 1a shows a typical temperature-induced exchange with varying concentrations of SDBS. In each case, a solution of DNA-CNT hybrids was incubated with a known amount of SDBS for 10 min. A final absorption spectrum was taken in the region of the E_{11} peak for (6,5) CNTs so that its shift due to a change in its local environment could be monitored. The data show a progressively increasing shift in the absorbance peak with increasing SDBS concentration with two limiting cases representing the limits where CNTs are coated purely with DNA (990 nm) or purely with SDBS (978 nm).

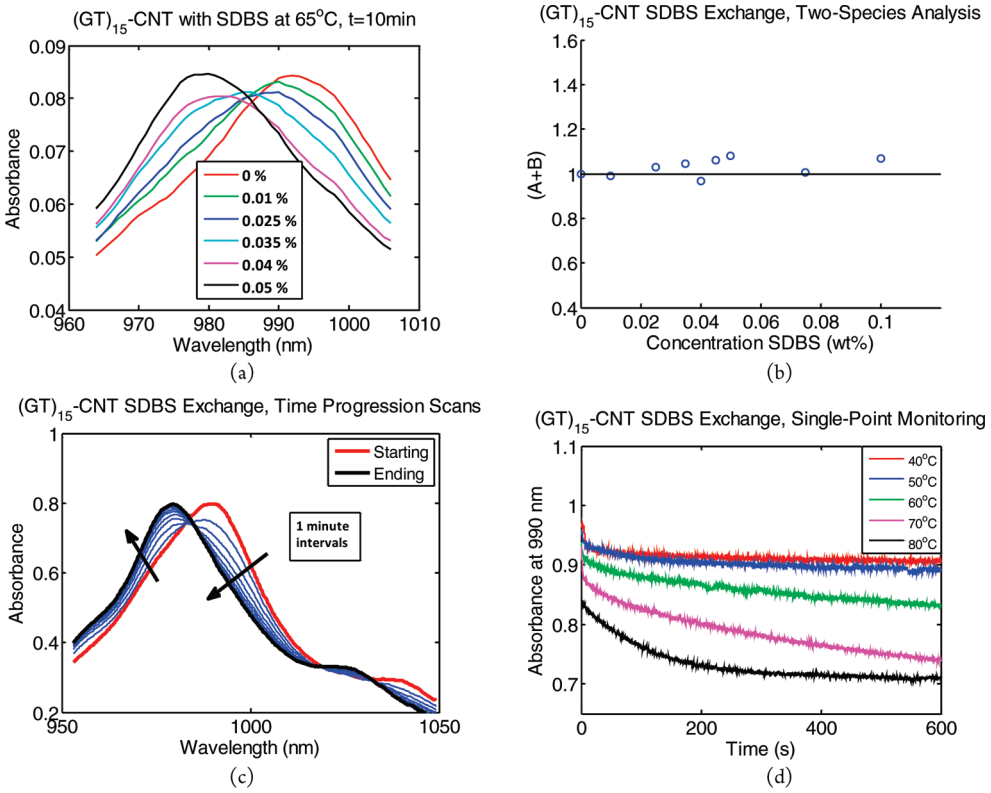

Figure 1. (a) Absorption spectra of $(GT)_{15}$/CNT hybrids after incubation for 10 min at various SDBS concentrations. We observe a systematic shift in the (6,5) E_{11} peak position. (b) Test in which intermediate stages of the reaction can be represented by a linear combination of the pure limiting species (DNA- or SDBS-coated CNTs, eq 2). $(A + B)$ should equal unity to be consistent with this hypothesis, where A and B are the prefactors from the fitted data. (c) Absorption spectra of $(GT)_{15}$/CNT hybrids incubated in 0.1 wt % SDBS at a constant temperature of 70 °C, showing a time-dependent shift in the concentrations of DNA-covered and SDBS-covered CNTs. (d) Raw data for temperature-dependent kinetics measured by the decay of the 990 nm absorption peak for $(GT)_{15}$/CNT hybrids. The data show a two-step mechanism with a quick initial change followed by a more gradual decrease. Note that data collection has stopped after 600 s, even though the completion of the reaction has not yet been reached (as clearly evident in 40C, 50C, and 60C samples).

3.1. Replacement of DNA by SDBS Can Be Monitored by Absorption Spectroscopy. Absorption data shown in Figure 1 could be interpreted in two ways: as a CNT population going from the limit of DNA-covered to SDBS-covered through a sequence of intermediate states or as a mixture of the two limiting states that retain their identities. In support of the latter of the two scenarios, imagine that the spectral curves given in Figure 1a represent a combination of two species (DNA-covered and SDBS-covered CNTs) rather than a series of intermediate species. We use a standard Lorentzian line shape

$$\Phi = \frac{a}{(b - x_0)^2 + a} + c \qquad (1)$$

to fit the absorbance line shape in the pure DNA-covered and SDBS-covered CNT limits. We then fit intermediate absorbance data by a linear combination of the two limiting functions,

$$\Phi_{\text{combined}} = A\left[\frac{a_1}{(b_1 - x_0)^2 + a_1{}^2}\right] + B\left[\frac{a_2}{(b_2 - x_0)^2 + a_2{}^2}\right] + c^1 \qquad (2)$$

thus representing the intermediate state as a combination of the two limiting states. Then a test of the hypothesis that intermediate compositions are linear combinations of the limiting ones is that A and B should add to 1. Figure 1b shows that this is indeed the case. (Regarding $A + B$ to be a random variable, we find the 95% confidence interval for the mean to be [0.998, 1.057], i.e., we can accept the hypothesis that $A + B = 1$ at this confidence level.)

Another way to conduct this type of experiment is to fix the SDBS concentration at a relatively high level (e.g., 0.1 wt %). Time evolution absorbance scans then show a progressive shift, presumably correlated again with an exchange of adsorbed chemical species. Figure 1c shows an example of this process with absorbance scans in the wavelength range of 950−1050 nm at time intervals of 1 min. The absorbance at any position along the 950−1050 wavelength interval can be monitored as a function of time.

Notice in Figure 1a,c the presence of a wavelength at which absorbance does not change as DNA is exchanged for SDBS. This further supports the hypothesis that absorbance in the intermediate stages when DNA/CNTs have been partially replaced by SDBS/CNTs is well represented as a linear mixture of pure SDBS- and DNA-coated spectra over a wide range of time and SDBS concentration. Specifically, this pivot point corresponds to the value of x_o (the wavelength) at which the absorbance of the two pure species is the same. Clearly, the absorbance at this wavelength would remain unchanged if intermediate compositions were linear combinations of the pure species. It can be found by taking the derivative of eq 2 (where $B = 1 - A$) with respect to A; in Figure 1c, the pivot point can be

dx.doi.org/10.1021/la2007793 |*Langmuir* 2011, 27, 8282–8293

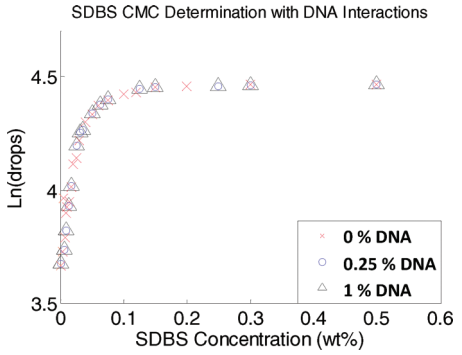

Figure 2. Determination of surfactant cmc and evaluation of possible interactions with free DNA for SDBS. SDBS appears not to have any significant interaction with free ssDNA over the range of concentrations examined.

seen at ~982 nm.

$$\frac{d\Phi}{dA} = \frac{a_1}{(b_1 - x_0)^2 + a_2{}^2} + \frac{a_2}{(b_2 - x_0)^2 + a_2{}^2} = 0 \qquad (3)$$

Because $(A + B)$ in eq 2 sum to unity, the reaction can be followed by tracking the evolution of absorbance at a convenient wavelength, say at 990 nm, Abs_{990}, as shown in Figure 1d. Provisionally, we adopt the hypothesis that any given CNT is covered entirely by DNA or entirely by SDBS. The effect of the CNT length on the kinetics of surfactant exchange, presented later, is consistent with this hypothesis; it would also explain why the absorption spectra are very well represented as a mixture of two pure species.

3.2. DNA/Surfactant Exchange Is a Kinetically Limited Reaction. Under the conditions reported in this article, we find that the replacement of DNA by SDBS can be written as the reaction

$$\text{DNA} - \text{CNT} + n\text{SDBS} \xrightarrow{k} \text{SDBS} - \text{CNT} + m\text{DNA} \qquad (4)$$

which proceeds to the right at a rate $k(T)$ that is independent of the free DNA concentration. To confirm this, we measured the kinetics as SDBS was kept at a relatively high concentration and the concentration of free DNA in solution was varied. Rough estimates suggest that a 7:1 weight ratio of SDBS is needed to coat the CNT surface completely;[44] all of the presented exchange experiments were kept at a 100:1 SDBS/CNT weight ratio (0.1 wt %). We found that the concentration of free DNA at concentrations of up to 0.3 wt % did not affect the rate at which SDBS displaced DNA on the CNT, thus leading to the interpretation that if there is enough SDBS to coat the CNTs then full exchange will take place. A second important conclusion is that the process is kinetic, not an equilibrium adsorption process. (See Supporting Information section S4 for data.)

3.3. Interaction between DNA and SDBS in Solution Can Be Neglected. To show that SDBS does not form complex and kinetics-altering structures with single-stranded DNA, surface tension measurements were performed. A simple drop counting method using a syringe was employed to estimate the surface tension.[42] For a fixed volume and tip area, the number of drops will increase as the surface tension of the solution decreases. For surfactants, the number of drops will reach a plateau value at the cmc. This serves as the threshold beyond which any additional added surfactant forms micelles and does not affect the surface tension of the solution. In Figure 2, the number of drops is plotted as a function of SDBS concentration for three different concentrations of free DNA. The overlapping data suggests that at these surfactant and DNA concentrations, interactions between the two are negligible. The cmc value can be estimated for the given experimental conditions as the concentration at which the curve attains a constant value, ~0.15 wt % SDBS. We conclude that (a) the interaction between DNA and SDBS can be neglected, which helps to simplify the surfactant exchange process to a quasi-first-order chemical reaction and (b) we can find surfactant concentrations below the cmc, where the surfactant is exchanged for the DNA in a reasonable time.

3.4. DNA/Surfactant Exchange Occurs in Two Stages. Figure 1d shows typical data on the time-dependent decay in absorbance at 990 nm for $(GT)_{15}$/CNT hybrids incubated in 0.1% SDBS at different temperatures. We notice a rapid initial drop in absorbance lasting no more than 3 s. (All of the solutions started at an absorbance of 1 ± 0.01.) We show later that this initial drop varies strongly and systematically by the DNA sequence type and temperature. There is a second process that proceeds at a slower pace, with a characteristic exponential decay. (See Supporting Information section S6 for detailed data.) To analyze these experimental data quantitatively, we introduce a two-step sequential mechanism for the interaction of SDBS with the DNA-CNT hybrid. A working hypothesis for the physical basis of a two-step process is sketched in Figure 3.

Data presented in section 3.1 and the length effect reported in section 3.5 both suggest that the dispersion consists of CNTs each coated entirely by either DNA or SDBS. This, in turn, suggests that DNA removal is a rapid process and the rate-limiting step is the formation of a defect in the coating. We propose that some fraction of the population of DNA-CNT has at least one defect; others are defect-free. Stage 1, then, corresponds to the rapid removal of DNA from those that initially have at least one defect. Stage 2 corresponds to the thermally activated formation of defects in the initially defect-free DNA-CNT rods. The initial drop in absorbance was found to be independent of the free DNA concentration in solution, leading to the interpretation that defects are due to local disorder in the DNA strand arrangement rather than the entire DNA strands coming off of the CNT; see Supporting Information section S8 for more details.

As a measure of the extent of the reaction, we monitor Abs_{990} and represent it by the additive combination

$$Abs_{990} = A_o(a_1 + a_2 e^{-t/\tau_2}) \qquad (5)$$

where A_o is the initial absorbance of the dispersion, which we maintain as unity. Stage 1 occurs immediately upon addition of the DNA-CNT dispersion to the preheated SDBS solution. Stage 2 begins with an absorbance of $Abs_{990} = A_o(a_1 + a_2)$ and asymptotically approaches $Abs_{990} = A_o a_1$, where $0 \le a_1, a_2 \le 1$, and $(a_1 + a_2) \le 1$. The decay of absorbance in the second step follows the exponential decay assumed in eq 5 (Supporting Information S6). This suggests that our reaction (eq 4) operates as a first-order or pseudo-first-order reaction, where the rate depends on [DNA-CNT] and [SDBS] is kept in excess. Because the timescales of the two stages are drastically different, we propose to analyze each step of the mechanism separately.

To confirm that the reaction is operating under a sufficient excess of SDBS when it is at a concentration of 0.1%, we compare in Figure 4 the kinetics of stage 2 under this condition with

dx.doi.org/10.1021/la2007793 |*Langmuir* 2011, 27, 8282–8293

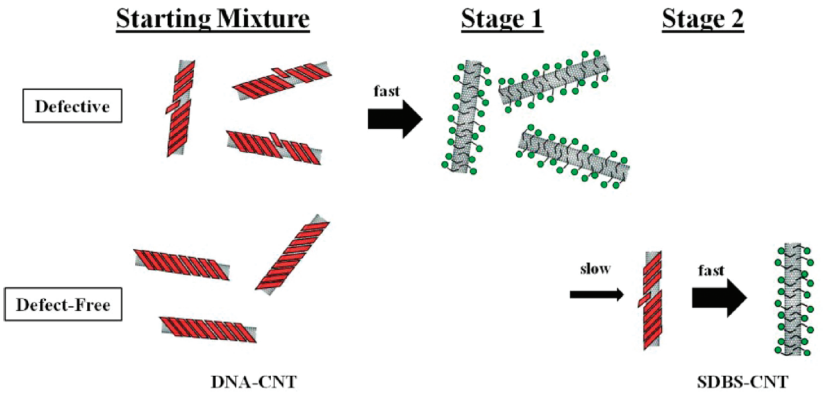

Figure 3. Schematic drawing illustrating the process of exchanging DNA for SDBS on the surfaces of CNTs. A two-step mechanism is proposed, consistent with observed data. As a working hypothesis, we propose that in stage 1, SDBS rapidly adsorbs onto CNTs with defects in the DNA coating. DNA is quickly displaced from the CNT. In stage 2, the subsequent removal of DNA from (initially) defect-free CNTs is limited by the rate of formation of new defects.

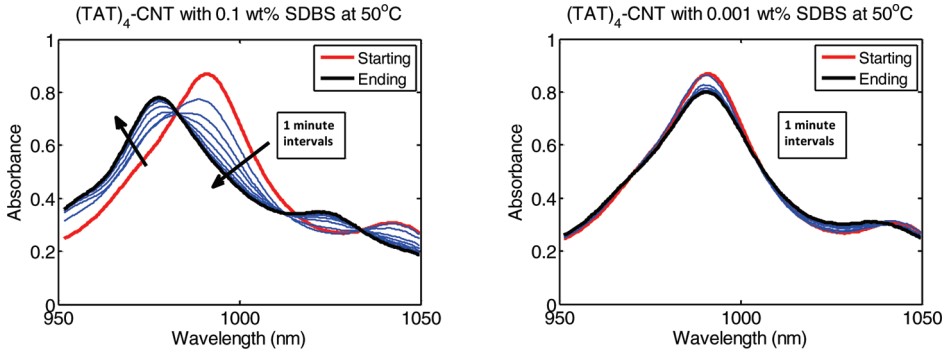

Figure 4. $(TAT)_4$/CNT hybrids under incubation with (a) 0.1 wt % and (b) 0.001 wt % SDBS at 50 °C. The higher concentration of SDBS results in the full coverage of CNTs, and a complete shift is seen. At the lower concentration, the transformation of DNA-CNT to SDBS-CNT stops as SDBS is depleted.

another experiment with concentration lower than the 7:1 weight ratio with CNTs expected to be insufficient for a full coverage of all CNTs. For a concentration of SDBS sufficiently high to be in excess, a full shift in the E_{11} peak position can be seen. At the lowered concentration, attenuation of the 990 nm peak stops after 10 min because SDBS falls below the reported 7:1 weight ratio and is no longer in excess.

We have also found that the reaction rate increases linearly with SDBS concentration (SI S9) so that the rate of reaction (eq 4) can be written as

$$\frac{d[\mathrm{DNA-CNT}]}{dt} = -k^1[\mathrm{DNA-CNT}][\mathrm{SDBS}] \qquad (6)$$

When SDBS is present in sufficient excess, as is the case for experiments reported in the remainder of this article, it can fully coat all of the CNTs without a significant loss of concentration in the bulk. Then, [SDBS] is absorbed into the rate constant, and if [SDBS] is held fixed, then [DNA-CNT] decays exponentially in time, as observed experimentally. The fact that the rate of reaction is linear in [SDBS] implies that the stoichiometric ratio between a DNA-CNT rod and SDBS is 1:1, suggesting that the activated-state limiting reaction rate consists of a single SDBS molecule invading a defect in the DNA coating on the CNT. (See SI section S9 for a more detailed discussion of how the two-step process in stage 2 drawn in Figure 3 results in the observed kinetics represented by eq 6).

3.5. Rate of Reaction Increases with CNT Length, Suggesting That DNA Removal on a Single CNT is Limited by the Nucleation of a Defect. Consider a series of samples each with the same total CNT length but with different average lengths of CNT fragments (Figure 5a). Experimentally, the fixed total length of CNT corresponds to a fixed starting absorbance, as we maintain in our experiments. Different average lengths of individual CNTs can be selected by choosing different SEC fragments.

We imagine that in stage 2 the substitution of DNA by SDBS will generally first require a nucleation step, perhaps a defect in the DNA coating large enough to admit the adsorption of some SDBS, followed by the progressive growth of this region as SDBS molecules replace DNA. For ease, think of a nucleation site as a chink in the DNA armor where SDBS molecules could potentially invade. The overall observed rate of removal will be limited by the slower of the two processes. Two limiting cases would be (a) nucleation rate $\gg$ growth rate and (b) nucleation rate $\ll$ growth rate. Furthermore, we can imagine two limiting cases for nucleation sites: heterogeneously only at the CNT ends or homogeneously throughout the length of the CNT. Together, these give us four limiting possibilities:

dx.doi.org/10.1021/la2007793 |*Langmuir* 2011, 27, 8282–8293

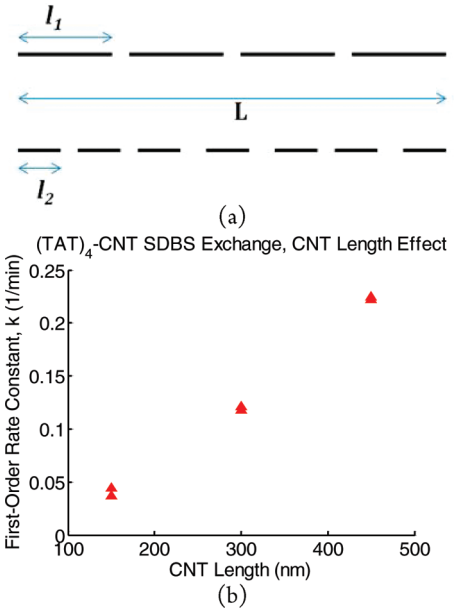

Figure 5. (a) Schematic drawing depicting two cases, each with a total CNT length of L but with different average individual CNT lengths l_1 and l_2. (b) Stage 2 kinetics for $(TAT)_4$ at 30 °C as a function of the average CNT length (l).

1 Nucleation rate ≫ growth rate with nucleation only at the CNT ends. DNA removal begins simultaneously at all CNT ends. The rate of the reaction (eq 6) will be proportional to the number of fragments, L/l (i.e., the kinetics would be more rapid for samples with shorter CNTs, in inverse proportion to their length).
2 Nucleation rate ≪ growth rate with nucleation only at CNT ends. The DNA removal rate is governed by the nucleation of defects at the CNT ends. The number of nucleation events is proportional to L/l, and the rate goes as $L/l \times l$ and thus is independent of the CNT length.
3 Nucleation rate ≫ growth rate with homogeneous nucleation sites along the CNT length. In this case, defects nucleate rapidly and DNA is removed at a characteristic rate. Neither process depends on the CNT length, so the kinetics would be expected to be independent of the CNT length.
4 Nucleation rate ≪ growth rate with homogeneous nucleation sites along the CNT length. The nucleation rate is proportional to the total length of CNT in the sample, L. However, because the growth is rapid, each nucleation event results in the conversion of one CNT. The rate of DNA removal is then proportional to the rate of nucleation (independent of CNT length) times the length of each CNT, l. Because L is held constant, the rate of removal is linear in CNT length.

Figure 5b shows that the kinetics, as measured by the first-order rate constant, depends strongly on the CNT length, increasing approximately linearly with it, consistent with the fourth hypothesis just cited. (See Supporting Information S11 for additional data.) That is, DNA removal appears to be limited by the homogeneous nucleation of defects on the CNT sidewall followed by the rapid substitution of DNA by SDBS. Note that this hypothesis then also explains why (a) intermediate states in stage 2 are represented well as a mixture of pure SDBS and DNA-coated CNTs, and (b) the kinetics depends linearly on the SDBS concentration. It also suggests that a starting DNA-CNT dispersion is composed of some with and others without a pre-existing defect. Those with a defect are converted rapidly in stage 1 to SDBS-coated CNTs; the remaining are converted in stage 2 at a rate limited by the nucleation of new defects.

This means that the rate of conversion of DNA-CNT to SDBS/CNT (in units of CNT length) is

$$\frac{d[DNA-CNT]}{dt} = -\frac{dN}{dt}l \qquad (7)$$

where dN/dt is the rate of defect nucleation. The nucleation rate, in turn, depends on the concentration of SDBS, the remaining length of DNA-coated CNTs ([DNA-CNT]), and a reference frequency, ν, per unit CNT length per SDBS concentration:

$$\frac{dN}{dt} = \nu[DNA-CNT][SDBS] \qquad (8)$$

The reference frequency contains a Boltzmann factor in the free energy of an activation free energy, which will be introduced in the following section. Combining eqs 6 and 8, we get

$$\frac{d[DNA-CNT]}{dt} = -\nu[DNA-CNT][SDBS] = -k[DNA-CNT] \qquad (9)$$

The first equality is identical in form to the experimentally observed form, eq 6, and additionally reveals the linear dependence of the rate of reaction on CNT length. The second equality is obtained if [SDBS] is maintained at a constant excess value, as we do in the remainder of the article (0.1% by wt), and the CNT length is also held fixed (250−350 nm SEC fraction in the remainder of the article).

From this, we can support two hypotheses distinguishing stage 1 and stage 2. These are that the first stage arises from defects (nucleation sites) in the structure that SDBS attacks immediately. Stage 2, then, is the thermally activated stage in which new defects have to be created.

4. ANALYIS OF SURFACTANT EXCHANGE KINETICS

We begin by examining the first stage in the kinetics of surfactant exchange. Because the first stage occurs rapidly, we can extract only a single measure from this part of the experiment—the total decrease in adsorption before the second stage of the DNA removal process commences. We follow by analyzing the kinetics of the second stage in greater detail. Specifically, we use Eyring kinetics to extract activation enthalpies for different sequences. In subsequent sections, we examine the results of fluorescence studies.

4.1. Stage 1: Probing the Initial Coverage of DNA on CNT.

In this study, we have chosen to examine three families of DNA sequences. The first comprises the 30-mers: $(TAT)_{10}$, $(GT)_{15}$ and $(TATT)_7TA$. The second and third are based on sequences that recognize (6,5) CNTs: $(TAT)_4$ and $(CGT)_3C$ (as shown by Tu et al.[16]). Among the recognition sequences, families were made by subtracting or adding one to two bases. For example, surfactant exchange was performed on $(TAT)_3T$, $(TAT)_3TA$, $(TAT)_4$, $(TAT)_4T$, and $(TAT)_4TA$.

To characterize the quick first stage, initial concentrations of the DNA-covered CNTs were adjusted so that the absorbance of the E_{11} peak at 990 nm was 1 ± 0.01. Instead of scanning the entire wavelength range, we followed the decay of absorbance at

dx.doi.org/10.1021/la2007793 |Langmuir 2011, 27, 8282–8293

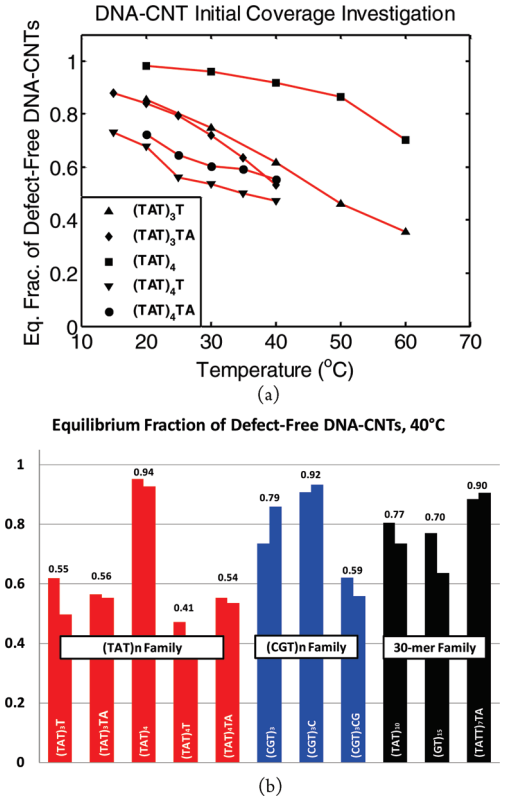

Figure 6. (a) Fraction of defect-free DNA-CNT for the $(TAT)_4$ family as a function of temperature. Significant nonmonotonic differences are observed between sequences of the same family. (b) Comparison of defect-free DNA-CNT fractions at 40 °C. Two runs were performed on each sequence with the average values reported above the columns. The two noticeable outliers, $(TAT)_4$ and $(CGT)_3C$, are the recognition sequences for the (6,5) CNT.

990 nm at short time intervals (e.g., Figure 1d). To determine the extent to which DNA-CNTs are converted at the end of stage 1, we extrapolated the second-stage kinetics to zero time. Figure 6 shows these intercept values for a variety of sequences as a function of temperature. We notice a strong nonmonotonic dependence on sequence length and an increase in stage 1 DNA-CNT conversion with increasing temperature.

As argued in section 3.4, we interpret stage 1 as the quick removal of DNA from the subpopulation of DNA-CNT that already has at least one nucleated defect on it. Because we are extracting the data at zero time, this measurement can be interpreted as the equilibrium fraction of DNA-CNTs without a defect, f_{nd}. In terms of the measured absorbance, it is estimated to be (eq 5)

$$f_{nd} = \frac{a_2}{(1 - a_1)} \tag{10}$$

The fraction of DNA-CNTs with at least one defect is $f_d = 1 - f_n^d$. For example, in an experiment, the second-stage kinetics for $(TAT)_4T$ had a zero-time intercept value of 0.84. The intensity of the 990 nm peak starts at 1.01 (fully DNA-covered, A_o) and ends at 0.71 (fully SDBS-covered). Therefore, $a_1 + a_2 = 0.84/1.01$, $a_1 = 0.71/1.01$, and the equilibrium fraction of defect-free DNA-CNTs is $f_{nd} = a_2/(1 - a_1) = 0.34 - 0.71/(1 - 0.71) = 0.43$.

Table 1. Free Energies, Enthalpies, and Entropies (along with Confidence Intervals, CI, of the Fit) of Defect Formation Extracted from the Fraction of DNA-CNT Converted to SDBS-CNT at the End of Stage 1

sequence	$\Delta H/k_BT$ (300 K) with 95% CI	$\Delta S/k_B$ with 95% CI	$\Delta G/k_B$
$(TAT)_3T$	19.4 ± 0.02	18.1 ± 0.02	1.3 ± 0.02
$(TAT)_3TA$	22.2 ± 0.10	21.1 ± 0.09	1.1 ± 0.1
$(TAT)_4$	24.2 ± 0.14	20.8 ± 0.12	3.4 ± 0.14
$(TAT)_4T$	13.6 ± 0.49	13.2 ± 0.48	0.4 ± 0.49
$(TAT)_4TA$	10.8 ± 0.43	10.2 ± 0.41	0.6 ± 0.43
$(CGT)_3$	18.0 ± 0.39	16.0 ± 0.35	2.0 ± 0.39
$(CGT)_3C$	22.1 ± 1.31	18.5 ± 1.09	3.7 ± 1.31
$(CGT)_3CG$	15.5 ± 0.16	14.5 ± 0.15	1.1 ± 0.16
$(GT)_{15}$	11.6 ± 0.50	9.6 ± 0.42	1.8 ± 0.5
$(TATT)_7TA$	17.3 ± 0.61	14.7 ± 0.51	2.6 ± 0.61
$(TAT)_{10}$	22.6 ± 0.35	20.4 ± 0.31	2.3 ± 0.35

Figure 6a plots the fraction of defect-free DNA-CNTs for a variety of sequences as a function of temperature. Figure 6b shows a more direct comparison between sequences at a given temperature of 40 °C. Within a family, we find significant nonmonotonic differences with sequence length. For example, both $(TAT)_4T$ and $(TAT)_3TA$ have significantly smaller fractions of defect-free DNA-CNT than does the recognition sequence $(TAT)_4$. Similarly, both $(CGT)_3$ and $(CGT)_3CG$ have significantly smaller fractions of defect-free DNA-CNT than does the recognition sequence $(CGT)_3C$. Let us interpret the fraction of defect-free DNA-CNT to result from the equilibrium

$$\text{DNA} - \text{CNT}_{\text{defect-free}} \overset{K_{eq}}{\Longleftrightarrow} \text{DNA} - \text{CNT}_{\text{defective}} \tag{11}$$

(Note that this is at fixed [SDBS]. Supporting Information S9 shows that the equilibrium depends on [SDBS].) Then, we can associate an equilibrium constant and free energy of defect formation, $\Delta G(T)$, as

$$K_{eq} = \frac{[\text{DNA} - \text{CNT}_{\text{defective}}]}{[\text{DNA} - \text{CNT}_{\text{defect-free}}]} = e^{-\Delta G/k_BT} = e^{-\Delta H/k_BT} e^{\Delta S/k_B} \tag{12}$$

$$\ln(K_{eq}) = \frac{-\Delta G}{k_BT} = \frac{-\Delta H}{k_BT} + \frac{\Delta S}{k_B} \tag{13}$$

These quantities are found from a linear plot of $\ln(K_{eq})$ versus $^1/_T$ and are reported in Table 1. (See Supporting Information section S10 for more information.)

Note again the differences among sequences of the same family ($(TAT)_4$ vs $(TAT)_4T$) and between sequences of the same length ($(GT)_{15}$ vs $(TAT)_{10}$). At 300 K, the free energy of defect formation in the recognition sequences, $(TAT)_4$ and $(CGT)_3C$, is some $2k_BT$ greater than for sequences that differ by only one base. This is consistent with our previous suggestion that recognition sequences have a more ordered structure as compared to related nonrecognition sequences.[16] Although we have not conducted a similar sequence-length comparison for the longer 30-mers, it is interesting that differences between sequences are somewhat attenuated compared to the shorter sequences. That is, it is not the absolute strength of binding but rather the difference in binding strength among related sequences and for related CNTs

dx.doi.org/10.1021/la2007793 |Langmuir 2011, 27, 8282–8293

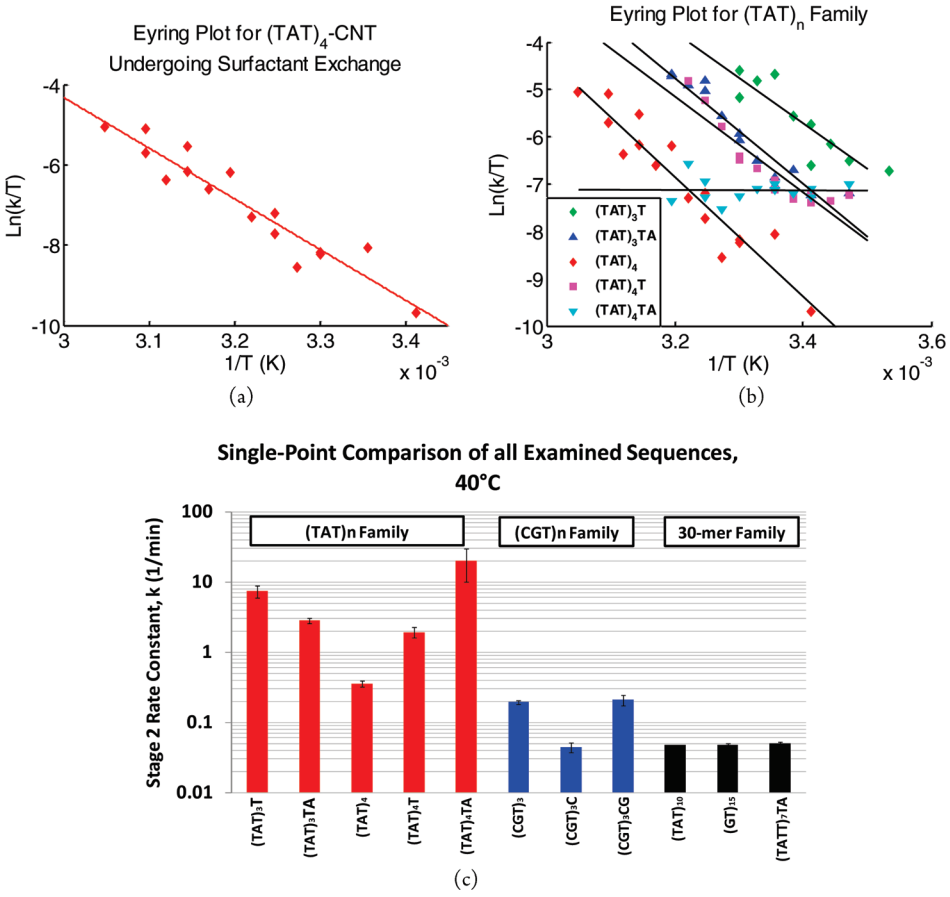

Figure 7. (a) Eyring plot of the rate constant, $\ln(k/T)$ vs $1/T$ enables the extraction of the activation enthalpy and relative entropy of the second-stage kinetics. Rate constants were calculated from the decay in absorbance at 990 nm, representing the DNA-covered/(6−5)-CNT E_{11} transition. (b) Eyring plots for the $(TAT)_n$ family of sequences. (c) Single-point comparison (at 40 °C) is shown, with the standard error demonstrating that DNA recognition sequences are stable compared to their compositional cousins.

(not studied here) that is responsible for the discriminating recognition shown by certain sequences. Note also the significantly larger magnitude of binding enthalpies compared to binding free energies. There is therefore some enthalpy−entropy compensation, which is discussed in Supporting Information S12. We ask the reader to keep these numbers in mind; the magnitudes of these values will be discussed in the following section because stages 1 and 2 relate to DNA-CNT binding strengths.

4.2. Stage 2: Analysis of DNA-Displacement Kinetics. To analyze the second step in the interaction between SDBS and DNA-CNT, we consider the reaction corresponding to the irreversible displacement of DNA by SDBS, eq 4, and the corresponding rate equations, eqs 6 and 9. That is,

$$\frac{[\mathrm{DNA-CNT}]}{[\mathrm{DNA-CNT}]_0} = \mathrm{e}^{-kt} \qquad (14)$$

Interpreting the rate constant using Eyring's activated rate theory[41] allows one to relate it to the activation enthalpy and entropy as

$$\ln\left(\frac{k}{T}\right) = \ln(\alpha) - \frac{\Delta H^{\ddagger}}{k_B T} + \frac{\Delta S^{\ddagger}}{k_B} \qquad (15)$$

where α is proportional to a rate, the length of CNTs, and [SDBS], as discussed in section 3.5. For the present purposes, this remains a constant quantity. The rate constant, k, is extracted by fitting the kinetics of the change in absorbance at different temperatures using eq 14. The activation enthalpy, $-\Delta H^{\ddagger}$, can be determined from the slope of $\ln(k/T)$ versus $1/T$. In principle, one could also obtain the absolute activation entropy, $\Delta S^{\ddagger}$, from the intercept except that the attempt rate prefactor contains many unknown (albeit constant) factors. However, if we make the (we feel, reasonable) assumption that the prefactor is the same for different DNA strands, then we can estimate differences in the activation entropy between different compositions. An example of such a plot is shown for $(TAT)_4$/CNT in Figure 7a. Figure 7b compares measurements within the $(TAT)_n$ family, and Eyring plots for $(CGT)_n$ and 30-mer families can be found in Supporting Information section S7.

Within the $(TAT)_n$ family of sequences, it is apparent that there is a strong and nonmonotonic dependence of the stage 2 reaction rate on the sequence, mirroring the results of stage 1. Figure 7c plots the rate constant at a fixed temperature (40 °C). The (6,5) recognition sequence, $(TAT)_4$, is removed at a rate that is about 20 times slower than for either $(TAT)_4T$ or $(TAT)_3TA$, both of which differ from it by only one base in length. Similarly, in the $(CGT)_n$ family, the recognition sequence, $(CGT)_3C$, is removed at a much slower rate than either of its compositional neighbors, $(CGT)_3CG$ and $(CGT)_3$. Along with the results of stage 2, this finding shows a strong relationship between recognition and binding strength. All sequences in the

dx.doi.org/10.1021/la2007793 |*Langmuir* 2011, 27, 8282–8293

Table 2. Activation Enthalpy with Entropy and Free-Energy Differences (with Respect to $(TAT)_4$) for Tested Sequences Obtained from Eyring Plot Linear Fits

sequence	$\Delta H^{\ddagger}/k_BT$ (300 K) with 95% CI	$\Delta(\Delta S^{\ddagger}/k_B)$ (subtracted from $(TAT)_4$) with 95% CI	$\Delta(\Delta G^{\ddagger})/k_BT$ (300 K, subtracted from $(TAT)_4$)
$(TAT)_3T$	32.2 ± 11.9	6.4 ± 12.1	3.4
$(TAT)_3TA$	37.4 ± 7.0	2.4 ± 7.6	2.3
$(TAT)_4$	42.1 ± 7.9		
$(TAT)_4T$	33.9 ± 9.7	6.2 ± 9.7	2.0
$(TAT)_4TA$	0 ± 6.2	40.7 ± 7.6	1.4
$(CGT)_3$	13.6 ± 2.6	27.9 ± 2.4	0.7
$(CGT)_3C$	23.5 ± 7.5	19.9 ± 6.7	−1.3
$(CGT)_3CG$	11.5 ± 7.1	29.9 ± 6.6	0.7
$(GT)_{15}$	17.7 ± 7.2	25.6 ± 6.5	−1.2
$(TATT)_{7.5}$	20.8 ± 5.4	22.0 ± 4.9	−0.7
$(TAT)_{10}$	23.1 ± 5.5	19.9 ± 6.4	−0.9

$(TAT)_n$ family have a similar slope in this plot (reflecting similar transition enthalpy) except for the sequence $(TAT)_4TA$, which presented behavior very unlike that of the other $(TAT)_n$ sequences. The near lack of a temperature dependence suggests a very small activation barrier, where the rate of reaction is governed almost entirely by the pre-exponential factor.

Note that the 30-mers are removed at a rate significantly slower than for the shorter DNA sequences, slower even than the special recognition sequences. As noted earlier, this suggests that the discriminative ability of the shorter sequences comes not so much from their absolute binding strength but from their differential binding. We showed earlier that, for a given DNA sequence, the kinetics increases linearly with CNT length, which we interpreted as a defect nucleation-limited mechanism. If, additionally, we imagine that defects are likely to nucleate near the ends of DNA strands, then we surmise that the number of nucleation sites and hence the nucleation rate are inversely proportional to the DNA length. If, somehow, there is an effective ligating effect between short strands on the CNT, then the number of nucleation sites can be greatly reduced (e.g., $(TAT)_4$ vs $(TAT)_4T$) and a short strand of DNA can behave more like that of a longer sequence.

Activation enthalpies and entropy differences, presumably representing the amount of energy required to elevate a particular "activation unit" from an absorbed to a transition state (TS), were extracted from the fitted data and are summarized in Table 2. Also shown are activation free-energy differences using $(TAT)_4$ as a reference. It is interesting that these differences are comparable to those found by an analysis of stage 1 data, supporting our hypothesis that stage 1 represents an equilibrium concentration of defective DNA-CNT and that stage 2 represents the kinetics of nucleation of defects in initially defect-free DNA-CNTs. Although at this point the identity of the TS unit is unknown, we can assume that the TS of the reaction is the point at which one or a few DNA bases are just slightly lifted before SDBS or even water can get into the created space to solvate them. Activation energies can be compared to experimentally documented DNA base free energies in an attempt to pinpoint the TS unit. Additionally, the conformational entropy loss for changing the conformation of single-stranded DNA from a random coil to an outstretched chain can be estimated to be

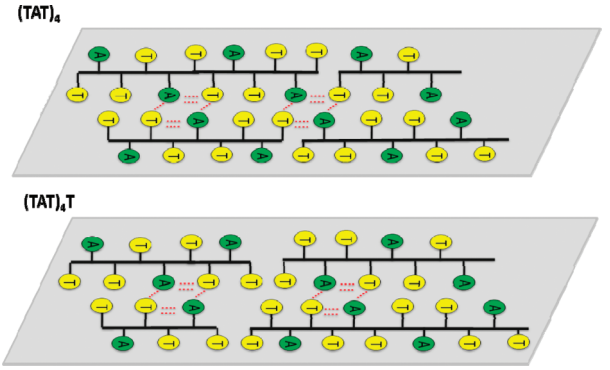

Figure 8. Proposed model to explain differences between $(TAT)_4$ and its relatives. The stability may increase for sequences with the ability to ligate the ends of adjoining strands through hydrogen bonds and AT-quartet formation.

k_BT/Kuhn length.[19,45] For ssDNA in a 10 mM ionic solution, the Kuhn length is roughly 5 nm, corresponding to seven or eight nucleotides.[19,46] Because the TS unit is likely composed of only a few DNA bases, the conformational activation entropies will all be far less than k_BT.

Extracted enthalpic values are $\sim(10-40)k_BT$. The lower end of this range well matches the measured free energy of DNA base−graphite binding found through single-molecule peeling experiments of $\sim(8-11)k_BT$/base,[35] suggesting that the transition-state unit in these cases could involve a single base. The larger numbers could imply that a greater number of bases are desorbed at the transition state or that additional interactions, such as hydrogen bonding between DNA bases, are involved.[16,17] In vacuum, a hydrogen bond between two DNA bases can be as much as $\sim10.9k_BT$/bond but is only $\sim3.4k_BT$/bond in a fully solvated state.[47,48] Because only half of the base is solvated when adsorbed onto graphite or a CNT, the actual energy of a hydrogen bond will be somewhere in between these two values. Because the observed TS activation energies appear to be closer to that of a single base than full strand adsorption energies, we propose a TS unit composed of one or two bases with the possible breaking of hydrogen bonds being the distinguishing property.

On the basis of molecular simulations, we have previously proposed a novel ordered DNA β-barrel structure stabilized by non-Watson−Crick hydrogen bonding between bases on adjacent DNA strands.[18] An example germane to the $(TAT)_n$ family is the possible formation of AT quartets that are bound together by six hydrogen bonds.[24] A transition state requiring the removal of one or two of the bases would require the breaking of six hydrogen bonds, and activation enthalpies would approach those found in a structure such as $(TAT)_4$. The presence or lack of such hydrogen bonding at the ends of the strands might account for the strong sequence specificity (Figure 8). The activated state then likely consists of the partial removal of one or two bases, which involves an increase in the free energy because initially there will not be enough space for water or SDBS to insert itself. SDBS, consisting of a benzene ring attached to a hydrocarbon tail, can be crudely estimated to be the same size as, if not slightly larger than, one "mer" of DNA, consistent with the assumption that the TS unit consists of one or two DNA bases. For the sake of argument, let us assume that the transition state is the same for all sequences (one to two bases slightly lifted up) and that differences in the activation free energy arise from the nature

of the structure of the DNA-CNT that needs to be disrupted. For example, if the DNA molecules are adsorbed as random coils interacting only by steric exclusion of each other, then we expect the main contribution to the activation enthalpy to come from base-stacking interactions. However, if the DNA strands are interacting with each other via hydrogen bonds, then their disruption will contribute to the activation energy.

Why might there be differences between sequences, both by composition (e.g., $(GT)_{30}$ vs $(TAT)_{10}$) and by length within a sequence family (e.g., $(TAT)_4$ vs $(TAT)_4T$)? Again, we propose that the activated state likely does not distinguish strongly between sequence composition and length. Therefore, we seek the difference in the nature of the DNA adsorbed state. To explain compositional differences of thermodynamic values in strands of the same length, examine the difference between $(GT)_{15}$ and $(TATT)_7TA$. Generally, purine bases, because of their two aromatic rings, have a higher affinity for adsorbing on a hydrophobic surface.[48] Purely by this comparison, $(GT)_{15}$ should have a higher affinity and thus slower removal kinetics than sequences such as $(TATT)_7TA$ and $(TAT)_{10}$. This is indeed not the case because the $\Delta H^{\ddagger}$value for $(GT)_{15}$ is within the error of the other 30-mer sequences tested. We propose that hydrogen bonding will then account for the differences seen. A sequence such as $(GT)_{15}$ is able to form G quartets on the surface of a CNT,[18] and $(TATT)_7TA$ may form AT quartets. The ability and frequency of quartet formation, bringing about added stabilizing hydrogen bonds, is one hypothesis to explain the disparities.

Recall Table 1, which contains free-energy differences between defective and defect-free states of DNA-CNTs. These magnitudes of the values are comparable to activation free-energy differences measured for stage 2, which suggests that the TS unit (Table 2) is related to the unit reported in Table 1.

With regard to differences seen in the short recognition DNA sequences, we propose an extended hydrogen-bonding scheme connecting multiple strands of DNA together on the CNT surface (Figure 8). Shown as parallel strands on an unrolled CNT, consecutive strands may be able to ligate together to form DNA strands with effective lengths that are much longer than an individual strand. Hydrogen bonds and even AT-quartet formation[24] are proposed to play a vital role in DNA-CNT hybrid stability. Additionally, sequences that can hydrogen bond to a further extent should have a lower starting free energy.

4.2.1. Effect of Urea on DNA-SDBS Exchange. One hypothesis to explain the differences in the observed rate constants among sequences of a given length is the existence of extended inter-strand hydrogen bonding. If a particular sequence contains DNA bases that are able to hydrogen bond to a neighboring strand, then the hybrid stability should be greatly increased. A simple way to test this hypothesis is to introduce an agent that interferes with hydrogen bond acceptors and donors in nucleic acids. Urea has been used extensively in the past at concentrations in the range of 1−12 M to disrupt hydrogen bonding in the double-stranded DNA molecule. In Figure 9a,b, $(TAT)_4$/CNT hybrids are subjected to 0.1% SDBS at 35 °C with and without urea at a concentration of 3 M for 10 min of incubation. Notice the faster 990 nm peak decay in the solution containing urea, suggesting that the breaking of DNA base hydrogen bonds decreases the overall stability of the hybrid.

4.2.2. SEC vs Non-SEC Samples. All of the data presented so far are for samples subjected to size-exclusion chromatography using an HPLC instrument (section 2). In view of the strong length dependence of the kinetics, this process is critically

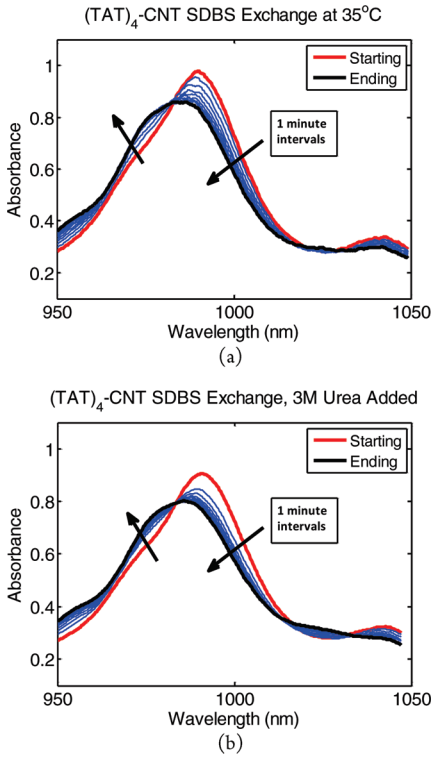

Figure 9. $(TAT)_4$/CNT hybrids, at a concentration equal to that used in section 3, were incubated with 0.1 wt % SDBS at 35 °C (a) without and (b) with 3 M urea for 10 min.

important. It also removes any impurities and free DNA in the sample. However, because ion-exchange (IEX) separations have often been conducted using samples that were not subjected to SEC separation and purification, it is pertinent to ask how the SEC process modifies the dispersion. We have observed that the recovery of the CNT sample can strongly depend on the DNA length (e.g., longer DNA strands have a higher recovery in the resulting SEC fractions). As a control experiment, we performed surfactant exchange on as-prepared samples prior to purification and length sorting by SEC. We find that these samples demonstrate quite different kinetics than their SEC counterparts. The $(TAT)_4$ non-SEC sample converted to SDBS-CNT an order of magnitude faster than its SEC version. Furthermore, $(TAT)_4T$ non-SEC conversion was a bit slower than that of the respective SEC sample and even slightly slower than the non-SEC recognition sequence $(TAT)_4$ (Supporting Information section S10). These results suggest that SEC sorting, which is critical to our experiments, modifies the population in DNA-CNT dispersions. SEC samples are of a controlled length, and non-SEC samples contain a broad range of lengths (100−500+ nm). The relatively low recovery after SEC suggests that this process removes a great number of poorly wrapped DNA-CNTs (greater than 90% of the hybrids), leaving only the "best" in the resulting fractions. This experiment further highlights the importance of careful sample preparation (i.e., the use of SEC in this instance) to obtain well-controlled starting samples.

5. FLUORESCENCE MEASUREMENTS ON (6,5) RECOGNITION SEQUENCES

In a parallel study, fluorescence spectroscopy was used to demonstrate the superior dispersing capability of the (6,5)

dx.doi.org/10.1021/la2007793 |*Langmuir* 2011, 27, 8282–8293

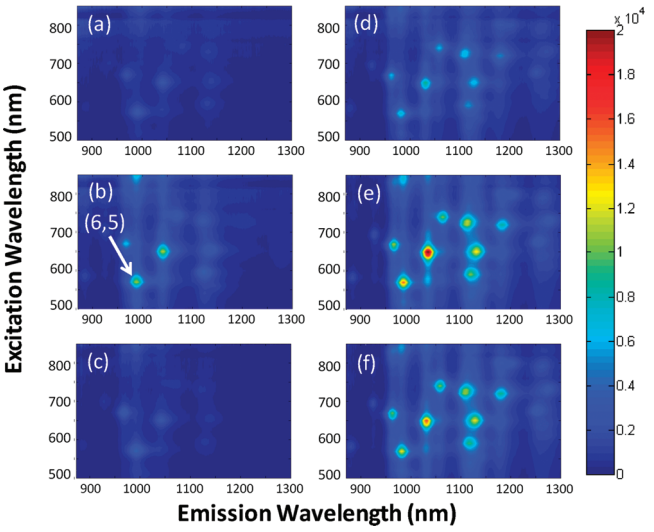

Figure 10. Two-dimensional photoluminescence map on (a, d) $(TAT)_3TA$, (b, e) $(TAT)_4$, and (c, f) $(TAT)_4T$-dispersed HiPco nanotubes. Samples a−c are in DNA, and samples d−f are measured in 1 wt % SDC.

recognition sequence, $(TAT)_4$. Three sequences, $(TAT)_3TA$, $(TAT)_4$, and $(TAT)_4T$, each differing from the others by only one DNA base, were used to disperse HiPCo tubes, followed by fluorescence spectroscopic analysis. HiPco tubes contain nanotube species with a broader range of diameters than CoMoCAT, which better helps to demonstrate the selectivity of the recognition sequences. A 2D fluorescence map can simultaneously provide spectral information for each semiconducting species in a sample, allowing the investigation of individual chirality nanotubes as well as the quality of the dispersion as a whole. From the fluorescence maps (Figure 10b), we find that nanotubes wrapped with $(TAT)_4$ are the brightest among the three samples (Figure 10a−c). There are multiple factors that could contribute to the brighter fluorescence of $(TAT)_4$. Besides the concentration of nanotubes, the fluorescence of carbon nanotubes is extremely sensitive to the environment, and different DNA sequences may adopt varied structures to influence the fluorescence intensity. To eliminate the effect of DNA wrapping on the fluorescence signals, DNA was replaced on the CNT surface by the addition of SDC to provide an equivalent environment for all nanotubes. SDC can effectively replace DNA on the nanotube surface and enhance the fluorescence of carbon nanotubes. After the addition of SDC (Figure 10d,e), the overall fluorescence intensities increased for all three samples. However, nanotubes in the sample initially dispersed by $(TAT)_4$ were still the brightest, indicative of the highest concentration of nanotubes present in the sample. Thus, it is reasonable to conclude that higher nanotube fluorescence signals in $(TAT)_4$ resulted from the better dispersion efficiency of the recognition sequence. It is possible that a stable structure of $(TAT)_4$ on the nanotube surface (e.g., Figure 8) allows a greater quantity of tubes to be dispersed. The dispersion efficiency is an important parameter in determining DNA sequences that support separation. Good dispersion efficiency is critical for effective separation. The fluorescence results complement the kinetic data on $(TAT)_4$, demonstrating its unique properties that enable nanotube purification.

6. CONCLUSIONS

In this study, we have investigated the DNA sequence-specific binding strength and selectivity for the (6,5) carbon nanotube. Using previously reported recognition DNA strands, a surfactant-exchange method was employed to explore quantitatively the differences among closely related sequences. Among certain families of short DNA strands (e.g., $(TAT)_3TA$, $(TAT)_4$, and $(TAT)_4T$), the correlation between the DNA-CNT binding strength and DNA length was nonmonotonic. The (6,5) recognition sequence $(TAT)_4$ was observed to bind ∼20 times stronger than either $(TAT)_3TA$ or $(TAT)_4T$, suggesting the formation of a stable secondary structure in the recognition sequence. Furthermore, a two-stage process was observed in which a certain fraction of DNA-CNTs, presumably with existing defects in their DNA coverage, were immediately exchanged with SDBS, followed by a slower process, presumably proceeding at a rate limited by time-dependent defect nucleation. Recognition sequences were found to have the lowest concentration of initially defective DNA-CNTs as well as the lowest rate constants for the subsequent kinetics of conversion. These data, coupled with 2D photoluminescence studies, shed light on the superior CNT dispersing capabilities of recognition DNA sequences. Other techniques, such as capillary electrophoresis (CE) or the direct imaging of individual tubes, may prove just as beneficial in determining DNA-CNT binding strengths and could be the subject of future research. In this study, we have focused on a single CNT chirality, (6,5). A natural follow-up study would be to examine the differential binding ability of a given DNA sequence on different CNT chiralities. It will also be interesting to attempt the direct monitoring of DNA dissociation from CNTs because this will confirm or dispute many of the hypotheses that have been formulated.

■ ASSOCIATED CONTENT

Ⓢ Supporting Information. Surfactant-exchange absorbance scans, free DNA control experiments, curve fitting, and data analysis. This material is available free of charge via the Internet at http://pubs.acs.org.

■ AUTHOR INFORMATION

Corresponding Author

*Phone: (610) 758-4396. E-mail: anj6@lehigh.

■ ACKNOWLEDGMENT

We acknowledge the assistance of Mr. Bryan Postelnek of Lehigh University and financial support from the National Science Foundation through grants CMS-0609050 and CMMI-1014960.

■ REFERENCES

(1) Ajayan, P. M. *Chem. Rev.* **1999**, *99*, 1787–1800.
(2) Baughman, R. H.; Zakhidov, A. A.; de Heer, W. A. *Science* **2002**, *297*, 787–792.
(3) Jorio, A.; Dresselhaus, G.; Dresselhaus, M. S. *Carbon Nanotubes, Advanced Topics in the Synthesis, Structure, Properties and Applications;* Springer: New York, 2008.
(4) Saito, R.; Dresselhaus, G.; Dresselhaus, M. S. *Physical Properties of Carbon Nanotubes;* Imperial College Press: London, 1999.
(5) Bahr, J. L.; Mikkelsen, E. T.; Bronikowski, M. J.; Smalley, R. E.; Tour, J. M. *Chem. Commun.* **2001**, 193–194.

(6) Furtado, C. A.; Kim, U. J.; Gutierrez, H. R.; Pan, L.; Dickey, E. C.; Eklund, P. C. *J. Am. Chem. Soc.* **2004**, *126*, 6095–6105.
(7) Bachilo, S. M.; Strano, M. S.; Kittrell, C.; Hauge, R. H.; Smalle, R. E.; Weisman, R. B. *Science* **2002**, *298*, 2361–2366.
(8) Moore, V. C.; Strano, M. S.; Haroz, E. H.; Hauge, R. H.; Smalley, R. E. *Nano Lett.* **2003**, *3*, 1379–1382.
(9) O'Connell, M. J.; Bachilo, S. M.; Huffman, C. B.; Moore, V. C.; Strano, M. S.; Haroz, E. H.; Rialon, K. L.; Boul, P. J.; Noon, W. H.; Kittrell, C.; Ma, J.; Hauge, R. H.; Weisman, R. B.; Smalley, R. E. *Science* **2002**, *297*, 593–596.
(10) Dieckmann, G. R.; Dalton, A. B.; Johnson, P. A.; Razal, J.; Chen, J.; Giordano, G. M.; Munoz, E.; Musselman, I. H.; Baughman, R. H.; Draper, R. K. *J. Am. Chem. Soc.* **2003**, *125*, 1770–1777.
(11) Kam, N. W. S.; Liu, Z.; Dai, H. *J. Am. Chem. Soc.* **2005**, *127*, 12492–12493.
(12) Kam, N. W. S.; O'Connell, M. J.; Wisdom, J. A.; Dai, H. *Proc. Natl. Acad. Sci. U.S.A.* **2005**, *102*, 11600–11605.
(13) Zheng, M.; Jagota, A.; Semke, E. D.; Diner, B. A.; Mclean, S. R. L.; Richardson, R. E.; Tassi, N. G. *Nat. Mater.* **2003**, *2*, 338–343.
(14) Huang, X.; Mclean, S. R. L.; Zheng, M. *Anal. Chem.* **2005**, *77*, 6225–6228.
(15) Zheng, M.; Jagota, A.; Strano, M. S.; Santos, A. P.; Barone, P.; Chou, S. G.; Diner, B. A.; Dresselhaus, M. S.; Mclean, S. R. L.; Onoa, G. B.; Samsonidze, G. G.; Semke, E. D.; Usrey, M.; Walls, D. J. *Science* **2003**, *302*, 1545–1548.
(16) Tu, X. M.; Manohar, S.; Jagota, A.; Zheng, M. *Nature* **2009**, *460*, 250–253.
(17) Khripin, C. Y.; Manohar, S.; Zheng, M.; Jagota, A. *J. Phys. Chem. C* **2009**, *113*, 13616–13621.
(18) Roxbury, D.; Manohar, S.; Jagota, A. *J. Phys. Chem. C* **2010**, *114*, 13267–13276.
(19) Manohar, S.; Tang, T.; Jagota, A. *J. Phys. Chem. C* **2007**, *111*, 17835–17845.
(20) McCarthy, B.; Coleman, J. N.; Czerw, R.; Dalton, A. B.; Panhuis, M. I. H.; Maiti, A.; Drury, A.; Bernier, P.; Nagy, J. B.; Lahr, B.; Byrne, H. J.; Carroll, D. L.; Blau, W. J. *J. Phys. Chem. B* **2002**, *106*, 2210–2216.
(21) Sowerby, S. J.; Cohn, C. A.; Heckl, W. M.; Holm, N. G. *Proc. Natl. Acad. Sci. U.S.A.* **2001**, *98*, 820–822.
(22) Sowerby, S. J.; Edelwirth, M.; Heckl, W. M. *J. Phys. Chem. B* **1998**, *102*, 5914–5922.
(23) Tao, N. J.; Shi, Z. *J. Phys. Chem.* **1994**, *98*, 1464–1471.
(24) Mamdouh, W.; Dong, M. D.; Xu, S. L.; Rauls, E.; Besenbacher, F. *J. Am. Chem. Soc.* **2006**, *128*, 13305–13311.
(25) Mamdouh, W.; Kelly, R. E. A.; Dong, M. D.; Kantorovich, L. N.; Besenbacher, F. *J. Am. Chem. Soc.* **2008**, *130*, 695–702.
(26) Sowerby, S. J.; Edelwirth, M.; Reiter, M.; Heckl, W. M. *Langmuir* **1998**, *14*, 5195–5202.
(27) Edelwirth, M.; Freund, J.; Sowerby, S. J.; Heckl, W. M. *Surf. Sci.* **1998**, *417*, 201–209.
(28) Sowerby, S. J.; Stockwell, P. A.; Heckl, W. M.; Petersen, G. B. *Origins Life Evol. Biospheres* **2000**, *30*, 81–99.
(29) Gu, J. D.; Leszczynski, J. *J. Phys. Chem. A* **2000**, *104*, 7353–7358.
(30) Otero, R.; Schock, M.; Molina, L. M.; Laegsgaard, E.; Stensgaard, I.; Hammer, B.; Besenbacher, F. *Angew. Chem., Int. Ed.* **2005**, *44*, 2270–2275.
(31) Xu, S. L.; Dong, M. D.; Rauls, E.; Otero, R.; Linderoth, T. R.; Besenbacher, F. *Nano Lett.* **2006**, *6*, 1434–1438.
(32) Johnson, A. T.; Johnson, C.; Klein, M. L. *Small* **2010**, *6*, 31–34.
(33) Manohar, S.; Mantz, A. R.; Bancroft, K. E.; Hui, C. Y.; Jagota, A.; Vezenov, D. V. *Nano Lett.* **2008**, *8*, 4365–4372.
(34) Shi, X.; Kong, Y.; Zhao, Y.; Gao, H. *Acta Mech. Sin.* **2005**, *21*, 249–256.
(35) Manohar, S. DNA-CNT Interactions. Ph.D. dissertation, Lehigh University, Lehigh, PA, 2010.
(36) Albertorio, F.; Hughes, M. E.; Golovchenko, J. A.; Branton, D. *Nanotechnology* **2009**, 20.
(37) Cathcart, H.; Nicolosi, V.; Hughes, J. M.; Blau, W. J.; Kelly, J. M.; Quinn, S. J.; Coleman, J. N. *J. Am. Chem. Soc.* **2008**, *130*, 12734–12744.
(38) Coleman, J. N. *Adv. Funct. Mater.* **2009**, *19*, 3680–3695.
(39) Islam, M. F.; Rojas, E.; Bergey, D. M.; Johnson, A. T.; Yodh, A. G. *Nano Lett.* **2003**, *3*, 269–273.
(40) Choi, J. H.; Strano, M. S. *Appl. Phys. Lett.* **2007**, *90*, 223114.
(41) Eyring, H. *Chem. Rev.* **1935**, *3*, 107–115.
(42) Chao, C. Y.; Carvajal, D.; Szleifer, I.; Shull, K. R. *Langmuir* **2008**, *24*, 2472–2478.
(43) Chou, S. G.; Ribeiro, H. B.; Barros, E. B.; Santos, A. P.; Nezich, D.; Samsonidze, G. G.; Fantini, C.; Pimenta, M. A.; Jorio, A.; Filho, F. P.; Dresselhaus, G.; Dresselhaus, M. S.; Saito, R.; Zheng, M.; Onoa, G. B.; Semke, E. D.; Swan, A. K.; Unlu, M. S.; Goldberg, B. B. *Chem. Phys. Lett.* **2004**, *397*, 296–301.
(44) Matarredona, O.; Rhoads, H.; Li, Z.; Harwell, J. H.; Balzano, L.; Resasco, D. E. *J. Phys. Chem. B* **2003**, *107*, 13357–13367.
(45) Bustamante, C.; Bryant, Z.; Smith, S. B. *Nature* **2003**, *421*, 423–427.
(46) Tinland, B.; Pluen, A.; Sturm, J.; Weill, G. *Macromolecules* **1997**, *30*, 5763–5765.
(47) Stofer, E.; Chipot, C.; Lavery, R. *J. Am. Chem. Soc.* **1999**, *121*, 9503–9508.
(48) Saenger, W. *Principles of Nucleic Acid Structure;* Springer-Verlag: New York, 1984.